Original Article
Propafenone suppresses esophageal cancer proliferation through inducing mitochondrial dysfunction

Wei-Bin Zheng, Yang-Jia Li, Yang Wang, Jie Yang, Can-Can Zheng, Xiao-Hui Huang, Bin Li, Qing-Yu He

Key Laboratory of Functional Protein Research of Guangdong Higher Education Institutes, Institute of Life and Health Engineering, College of Life Science and Technology, Jinan University, Guangzhou 510632, China

Abstract: Esophageal squamous cell carcinoma (ESCC) is one of the most common malignant tumors with poor survival and limited therapeutic options. The aim of this study is to identify novel anticancer strategies from existing Food and Drug Administration (FDA)-approved drugs that have been used to clinically treat other diseases. Here, propafenone, an antiarrhythmic medication, was found to induce apoptosis and exert a significantly inhibitory effect on the proliferation and colony-forming ability of ESCC cells in a dose-dependent manner without observed cytotoxicity on normal esophageal epithelial cells. Furthermore, propafenone markedly suppressed growth of tumor xenografts in nude mice by reducing the Ki-67 proliferation index and angiogenesis but did not damage the vital organs of the animals. Mechanistically, our data from the proteomics, Western blot and flow cytometry analyses demonstrated that propafenone caused mitochondrial dysfunction as indicated by a decreased mitochondrial membrane potential and reduced expression of Bcl-xL and Bcl-2. In summary, this study provides the first evidence that propafenone, an FDA-approved drug to treat arrhythmias, could be a novel therapeutic strategy for treating ESCC without obvious side effects.

Keywords: Drug repositioning, propafenone, apoptosis, mitochondria dysfunction, ESCC

Introduction

Esophageal squamous cell carcinoma (ESCC), a tumor of the digestive tract, has been ranked as the eighth most common cancer and the fifth leading cause of cancer-related deaths worldwide with poor overall survival [1]. Despite the great development of therapeutic regimens, the resistance of tumors to chemo- and radiotherapies leads to recurrence and poor prognosis of this lethal disease [2, 3]. Many the chemotherapeutic agents were found to possess serious adverse effects in addition to limited efficacy [4]. Therefore, there is an urgent need to invent novel therapeutic strategy.

In the field of drug discovery, the concept of "old drugs for new applications" is gaining increasing traction [5]. When a new function of a clinical drug is found, the drug could have much more opportunities for clinical use. Propafenone HCL, a Vaughan-Williams class IC antiarrhythmia medication [6], has been extensively applied to treat paroxysmal supraventricular

tachycardia, paroxysmal atrial fibrillation, and ventricular arrhythmia. The functions of propafenone in the treatment of arrhythmias could be explained by its activities in blocking beta-receptors and calcium channels [7]. However, the effects of propafenone in cancer were rarely reported, and the underlying mechanisms are largely unknown. In this study, *in vitro* and *in vivo* experiments were performed to provide evidence on the role of propafenone in cancer treatment. We found that propafenone elicited a strong ability to suppress the growth of ESCC cells *in vitro* and *in vivo*.

Quantitative proteomics is a systemic tool to uncover the mechanisms of anticancer compounds [8, 9]. Data-independent acquisition (DIA) mass spectrometry (MS) is a label-free quantification method that offers more consistent peptide detection and accurate proteome quantification [10]. A recent study used DIA-MS to screen and verify protein biomarkers in ESCC [11]. In the present study, DIA-MS coupled with bioinformatics was performed to elu-

cidate the molecular mechanisms involved in the anticancer effect of propafenone in ESCC cells. The proteomics data suggested that propafenone may induce apoptosis and inhibit cancer cell proliferation by causing mitochondrial dysfunction. Mitochondria, a dynamic cellular network of organelles, harbor the tricarboxylic acid (TCA) cycle and oxidative phosphorylation machinery to produce energy in the form of ATP [12]. Recent studies showed that mitochondria act as an important regulator of tumorigenesis, and its activity is strongly related to cancer development and progression [13]. Interestingly, mitochondria-mediated apoptosis, an intrinsic pathway of apoptosis, is activated when cancer cells are exposed to cell stress or damage, and several key molecules, including anti-apoptotic proteins Bcl-2 and Bcl-xL, are involved in this process [14, 15]. Thus, we aim to investigate the anticancer property of propafenone and to determine the significance of the mitochondrial pathway in this effect. The outcome of this study could prove the potential of propafenone, an FDA-approved antiarrhythmic medication, as a therapeutic strategy in the treatment of cancer.

Materials and methods

Cell lines and culture

The human ESCC cell lines KYSE30, KYSE150 and KYSE270 (obtained from DSMZ, Braunschweig, Germany) were cultured in RPMI 16-40 medium (Life Technologies, Gaithersburg, MD, USA) supplemented with 10% fetal bovine serum (FBS; Life Technologies) at 37°C in 5% CO_2.

Cell viability assay

Cell viability was measured by the WST-1 assay (Beyotime, Jiangsu, China) as described previously [8]. ESCC cells were seeded into 96-well plates and treated with propafenone at various concentrations for different duration. WST-1 was added and incubated at 37°C for 2 h, and then the absorbance was measured on an automated microplate spectrophotometer (Bio-Tek Instruments, Vermont, USA) at a wavelength of 450 nm.

Colony formation assay

A colony formation assay was performed as described previously [16]. In brief, ESCC cells were seeded into 6-well plates at a density of 3000 cells per well and treated with different concentrations of propafenone for 14 days. After washing twice with PBS, the plates were fixed with methanol for 15 min at room temperature and then stained with 1% crystal violet for 10 min. The number of colonies was counted, and all statistical measurements were obtained from three independent experiments.

Annexin V-FITC/PI staining assay

Cell apoptosis was determined by using an Annexin V-FITC/PI Apoptosis Detection kit (KeyGen, Jiangsu, China) [9]. Cells were suspended in binding buffer, stained with annexin V-FITC and propidium iodide (PI) for 15 min at room temperature in the dark. Apoptosis was assessed and analyzed by using a C6 flow cytometer (BD Biosciences, San Diego, CA, USA).

Measurement of the mitochondrial membrane potential

A JC-1 assay kit (Beyotime) was used to measure the mitochondrial membrane potential as described previously [17]. In brief, cells were collected after exposure to propafenone at various concentrations for 72 h, incubated with JC-1 (5 μg/ml) for 20 min at 37°C, and then rinsed twice with PBS. The cell resuspension was assayed by using a C6 flow cytometer to measure the JC-1 fluorescence intensities of red aggregates (hyperpolarization) and green fluorescence monomers (depolarization). The change in mitochondrial depolarization was calculated as the green/red fluorescence intensity ratio.

Western blot assay

Whole-cell lysates were prepared in lysis buffer (Cell Signaling Technology, Beverly, MA, USA) [18]. A BCA kit (Thermo Fisher Scientific, Waltham, MA, USA) was used to determine the protein concentration. The samples were loaded onto a sodium dodecyl sulfate (SDS)-PAGE gel and subsequently electrotransferred to a PVDF membrane (Millipore, Bedford, MA, USA). After blocking with 5% nonfat milk for 1 h, the membrane was incubated with primary antibodies for 2 h at room temperature and washed three times for 10 min per wash with 1x Tris-buffered saline with Tween (TBST). Next, the
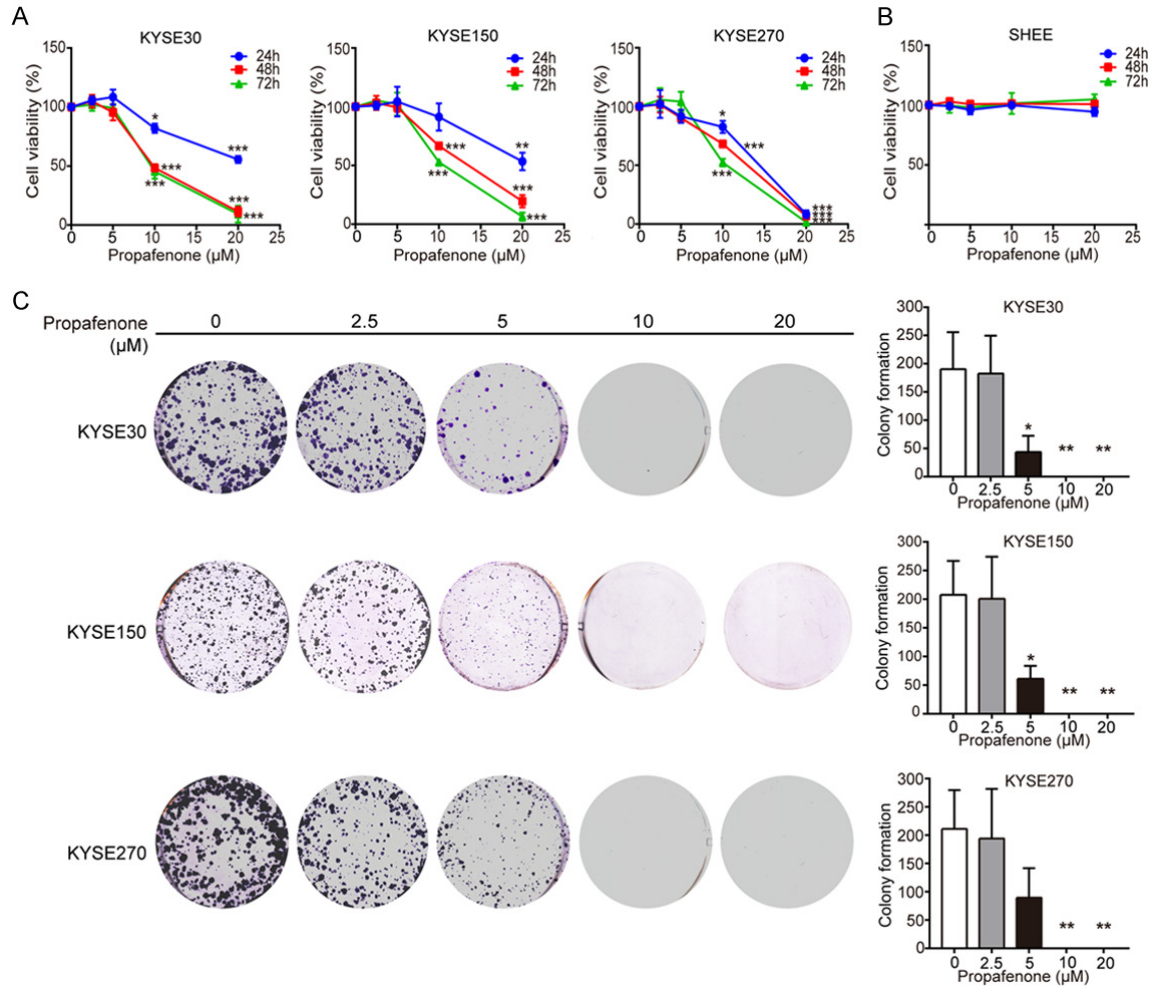
Figure 1. Propafenone inhibits ESCC cell proliferation. A. A WST-1 assay was performed to determine the cell viability of KYSE30, KYSE150, and KYSE270 cells treated with the indicated concentrations of propafenone for 24, 48 and 72 h. B. Propafenone did not affect the proliferation of the normal esophageal epithelial cell line SHEE. C. Propafenone inhibited the colony-forming ability of ESCC cells. Bars, SD; *, $P < 0.05$; **, $P < 0.01$; ***, $P < 0.001$ compared with control cells.

membrane was incubated with corresponding horseradish peroxidase (HRP)-conjugated secondary antibodies for 1 h at room temperature. The reaction was visualized using Clarity Western ECL substrate (Bio-Rad, Hercules, CA, USA) and detected by exposure to autoradiographic film [19]. The antibodies used targeted caspase-3, cleaved caspase-3, Bcl-2, Bax, ERK, p-ERK, and survivin (Cell Signaling Technology); Bcl-xL (Abcam, Cambridge, UK), and actin (from Santa Cruz Biotechnology, Santa Cruz, CA, USA).

MS and bioinformatics analyses

KYSE270 cells were treated for 10 μM propafenone for 72 h, and whole-cell lysates were homogenized in RIPA lysis buffer. After further trypsin digestion through the method of filter-aided sample preparation (FASP), the peptide samples were vacuum-freeze-dried and resuspended in anhydrous acetonitrile solution for further desalination with a MonoTIPTM C18 Pipette Tip (GL Sciences, Tokyo, Japan). Next, the peptides were analyzed with an Orbitrap Fusion Lumos mass spectrometer (Thermo Fisher Scientific). The raw data were searched using Proteome Discoverer (Thermo Fisher Scientific) and Spectronaut (Omicsolution Co., Ltd., Shanghai, China) software. An FDR of 1% was set to identify proteins. The differently expressed proteins were analyzed by Ingenuity Pathway Analysis (IPA, Ingenuity Systems, Redwood City, CA, USA) as described previously [8].
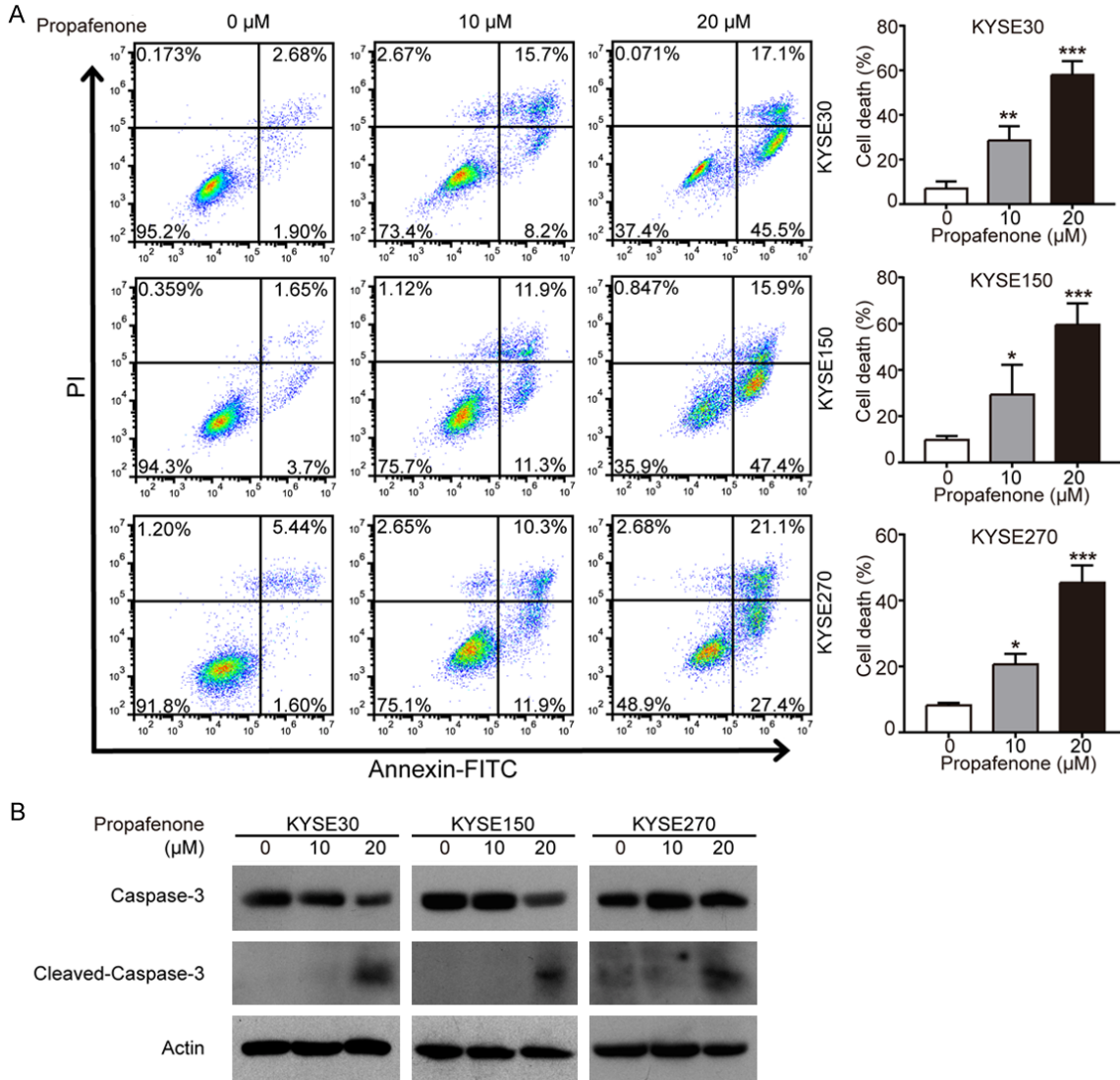
Figure 2. Propafenone induces apoptosis in ESCC cells. A, B. KYSE30, KYSE150, and KYSE270 cells were exposed to the indicated concentrations of propafenone (up to 20 μM) for 72 h, and apoptotic cells were determined with annexin V-FITC/PI double staining by flow cytometry (A), and Western blotting was performed to compare the expression levels of caspase-3 and cleaved caspase-3. Bars, SD; *, $P < 0.05$; **, $P < 0.01$; ***, $P < 0.001$ compared with control cells.

Tumor xenograft experiments

Female BALB/c nude mice aged 6-8 weeks were maintained under standard conditions and cared for according to the institutional guidelines for animal care. All the animal experiments were approved by the Ethics Committee for Animal Experiments of Jinan University. KYSE270 cells (5×10^5 cells in equal volumes of PBS and Matrigel) were subcutaneously implanted into the flanks of mice to establish tumor xenografts [20]. When the tumor xenografts reached 5 mm in diameter, the mice were randomly divided into treatment and control groups. The treatment groups received propafenone (10 mg/kg or 20 mg/kg) through intraperitoneal injection every other day, whereas the control group received vehicle only. The body weight of the mice was monitored weekly during the experiments to evaluate overall health. Tumor size was measured every three days, and the tumor volume was calculated using the following equation: $V = (\text{length} \times \text{width}^2)/2$. All animals were killed at the end of the study, and their tumors, lungs, liver, and kidneys were collected for further
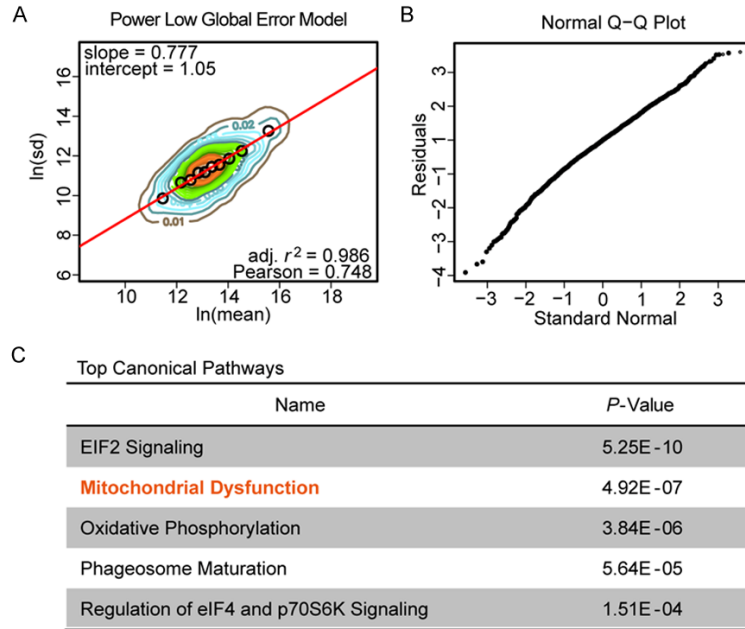
Figure 3. Proteomics analysis for the identification of the potential mechanism(s) of action of propafenone. A. PLGEM model using a regression fitting analysis with a contour plot; black circles showed a good fitting of the DIA-MS data by the PLGEM model. B. A Q-Q plot was used to detect a normal distribution of the residual standard deviations between the modeled and the determined data. C. The top five canonical pathways from the IPA analysis of differently expressed proteins in propafenone-treated cells.

creased cell proliferation over time and potently inhibited cell proliferation with increasing concentrations in KYSE30, KYSE150 and KYSE270 cells (**Figure 1A**). The cell viability decreased by half when ESCC cells were treated with 10 µM propafenone for 72 h. Of note, treatment with propafenone did not exert any toxic effects in normal esophageal epithelial cells (**Figure 1B**). In addition, we determined the effect of propafenone on the colony-forming ability of ESCC cells. As shown in **Figure 1C**, the number of colonies formed by ESCC cells was significantly reduced by propafenone in a dose-dependent manner. Taken together, these results suggest that propafenone has a tumor suppressive effect in ESCC.

Propafenone induces apoptosis in ESCC cells

Next, we studied the effect of propafenone on apoptosis in ESCC cells. ESCC cells were treated with different concentrations of propafenone (up to 20 µM), and an annexin V-FITC/PI double staining assay was performed using flow cytometric analysis. As shown in **Figure 2A**, a dose-dependent induction of apoptosis was observed in KYSE30, KYSE150 and KYSE270 cells treated with propafenone. The effect of propafenone on apoptosis was also evidenced by the increased expression levels of cleaved caspase-3 in propafenone-treated ESCC cells (**Figure 2B**). Collectively, these results indicated that propafenone can trigger apoptosis to inhibit cell proliferation in ESCC cells.

Proteomics analysis suggests the involvement of mitochondrial signaling in antitumor activity of propafenone in cancer cells

To quantify the proteomic alterations and elucidate the potential molecular mechanism of propafenone treatment on ESCC cells, we used DIA-MS, which has been justified as a good tool for protein quantitation, especially for low abundance proteins. Here, a total of 2799 pro-

analysis. Immunohistochemical analyses of the proliferative index and microvessel density (MVD) were performed using antibodies against Ki-67 (Dako, Mississauga, ON, Canada) and CD31 (Santa Cruz Biotechnology), respectively [21].

Statistical analysis

All *in vitro* experiments were performed in triplicate. GraphPad Prism software (San Diego, CA, USA) was used to calculate statistically significant differences with a Student's t-test method. All values were expressed as the means ± SD from three independent experiments. All statistical tests were two-sided, and $P < 0.05$ was considered statistically significant.

Results

Propafenone inhibits ESCC cell proliferation

To evaluate the inhibitory effect of propafenone on cancer cell proliferation, ESCC cells were exposed to various concentrations of propafenone for 24 h, 48 h and 72 h, and the results showed that propafenone gradually de-
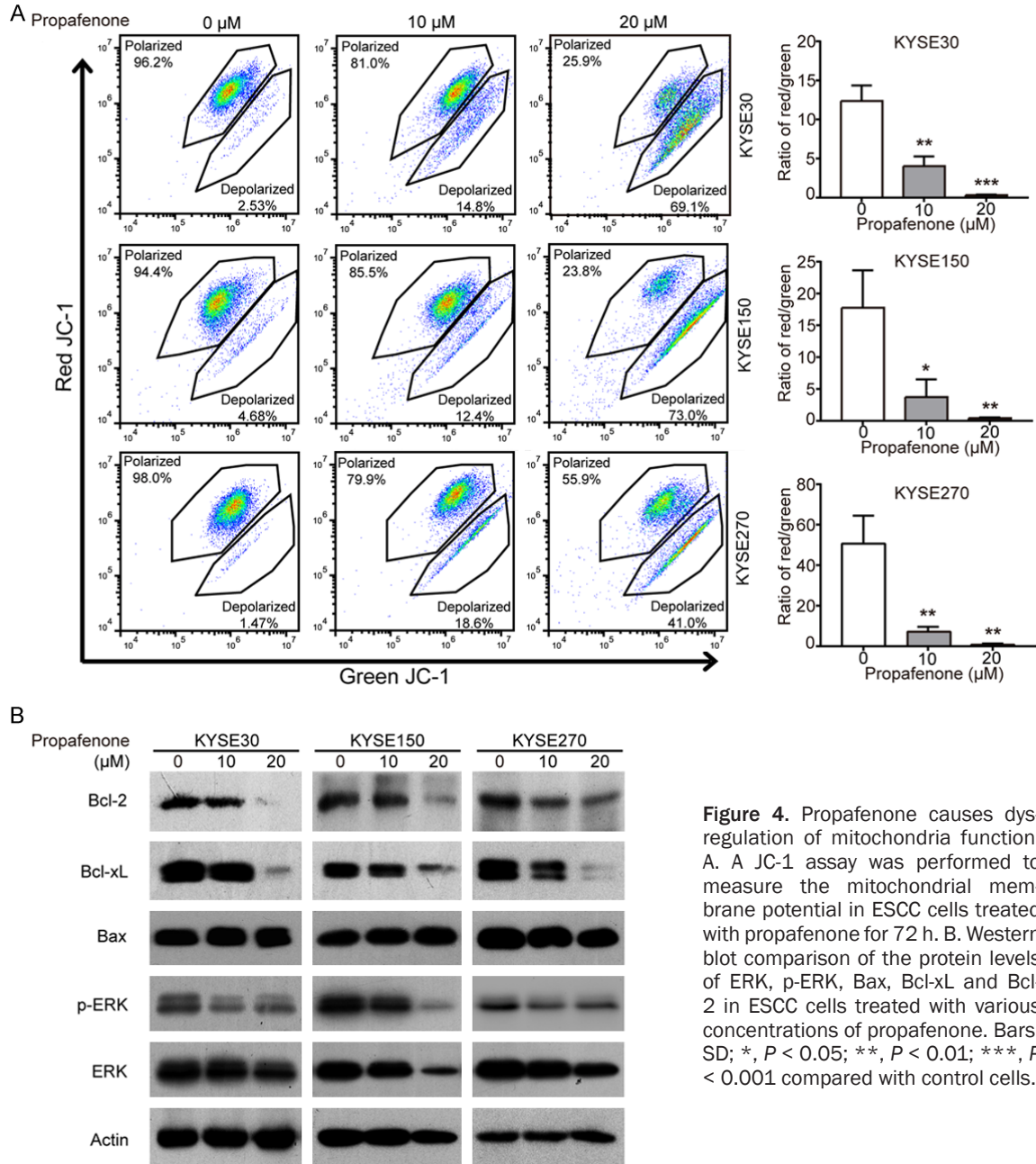
Figure 4. Propafenone causes dysregulation of mitochondria function. A. A JC-1 assay was performed to measure the mitochondrial membrane potential in ESCC cells treated with propafenone for 72 h. B. Western blot comparison of the protein levels of ERK, p-ERK, Bax, Bcl-xL and Bcl-2 in ESCC cells treated with various concentrations of propafenone. Bars, SD; *, $P < 0.05$; **, $P < 0.01$; ***, $P < 0.001$ compared with control cells.

teins were identified and quantified from the triplicate samples after propafenone treatment (10 µM for 72 h) against samples with DMSO treatment. Meanwhile, a total of 428 differentially expressed proteins (Supplementary Table 1) was identified through the power law global error model (PLGEM) algorithm [22], a statistical test for analyzing protein abundance, with a slope of 0.777 and an adjusted r^2 of 0.986 (Pearson r = 0.748) (**Figure 3A**). The quantile-quantile (Q-Q) plot presented that the data had a fitted normal distribution of the residual stan-dard deviations between the modeled and the actual values (**Figure 3B**). Next, to explore the molecular mechanism involved in the growth inhibition of propafenone in ESCC cells, we used IPA software to characterize the canonical pathways in which the differently expressed proteins participated. As shown in **Figure 3C**, we noticed that the signaling associated with mitochondrial dysfunction, one of the top five canonical pathways with P value of 5.92E-7, was significantly affected by propafenone treatment.

Propafenone causes dysregulation of mitochondria function

Based on the proteomics data above, we investigated effect of propafenone on mitochondria function. The integrity of mitochondrial membrane permeability was determined with the fluorescent dye JC-1, which fluoresces a red color in healthy mitochondria but a green color when mitochondria are damaged. KYSE30, KYSE150 and KYSE270 cells were treated with increasing concentrations of propafenone for 72 h and stained with JC-1. A dose-dependent decrease of the red/green fluorescence ratio was observed (**Figure 4A**), suggesting that propafenone may induce apoptosis through decreasing the mitochondrial membrane potential. Simultaneously, we detected the expression levels of proteins involved in the mitochondrial pathway. Western blot data showed that propafenone treatment significantly downregulated the expression levels of the anti-apoptotic proteins Bcl-xL and Bcl-2 in ESCC cells (**Figure 4B**). In addition, reduced expression of p-ERK was observed in propafenone-treated cells (**Figure 4B**), indicating the inactivation of the ERK signaling pathway, which has been reported to be an upstream regulator of Bcl-2 and Bcl-xL [23, 24]. Taken together, these results demonstrated that propafenone may induce apoptosis through the intrinsic (i.e., mitochondrial) pathway.

Propafenone suppresses tumor growth in vivo

Given that propafenone exerted a significant inhibitory effect on the proliferation of cancer cells, we next evaluated the therapeutic potential of propafenone using a mouse model. Propafenone was intraperitoneally injected into nude mice bearing established subcutaneous tumor xenografts, and its effect on tumor growth was monitored. The results showed that the tumor burden was markedly suppressed by propafenone treatment with a decrease of 69.2% in the group receiving 20 mg/kg propafenone (**Figure 5A**). As shown in **Figure 5B**, the immunohistochemical analysis of the Ki-67 proliferation index also provides evidence that tumor cell proliferation was significantly inhibited by propafenone (mean index decreased from 56.3 ± 6.7% in the DMSO-treated group to 20.7 ± 5.1% in the 10 mg/kg propafenone-treated group and 11.3 ± 4.0% in the 20

mg/kg propafenone-treated group). Furthermore, we investigated the effect of propafenone on tumor angiogenesis, and an analysis of microvessel density (indicated by CD31 staining) showed that treatment of propafenone resulted in a decrease in tumor angiogenesis (**Figure 5B**). Mechanistically, same with the in vitro data (**Figure 4B**), significant downregulation of Bcl-xL and Bcl-2 expression levels was observed in propafenone-treated tumors compared with those in the control group by Western blot (**Figure 5C**). No significant difference between the treated and control groups in terms of body weight was observed (**Figure 5D**). Histological examination of vital organs, including the lung, liver and kidneys, did not reveal any overt changes in morphology (**Figure 5E**), suggesting that propafenone treatment had no toxic effects on animals.

Discussion

Finding new functions for existing drugs, also known as "drug repositioning", is a promising approach for identifying more therapeutic strategies in translational and clinical studies [5]. Since FDA-approved drugs have clear descriptions of their physicochemical properties and pharmacokinetics as well as stronger evidence of drug safety, it may be a faster and more effective strategy to repurpose existing drugs for cancer treatment. Propafenone, a Vaughan-Williams class IC antiarrhythmic medication, is often used to manage atrial fibrillation and other supraventricular arrhythmias and has no severe side effects and a favorable drug tolerance [25, 26]. Several studies revealed that propafenone can block the activities of potent sodium channel and calcium channel signaling [27-30]. However, there are few reports on the implication of propafenone in the treatment of cancer. In our study, we found that propafenone triggered apoptosis and displayed a significantly inhibitory effect on the proliferation and colony-forming ability of ESCC cells in a dose-dependent manner (**Figure 1**). More importantly, the animal experiment demonstrated that propafenone markedly suppressed the growth of tumor xenografts in nude mice (**Figure 5**). It is worth noting that the dose used in our *in vivo* study, 120 mg every other day, is much lower than the recommended dose of propafenone (from 450 mg to 900 mg each day) for the
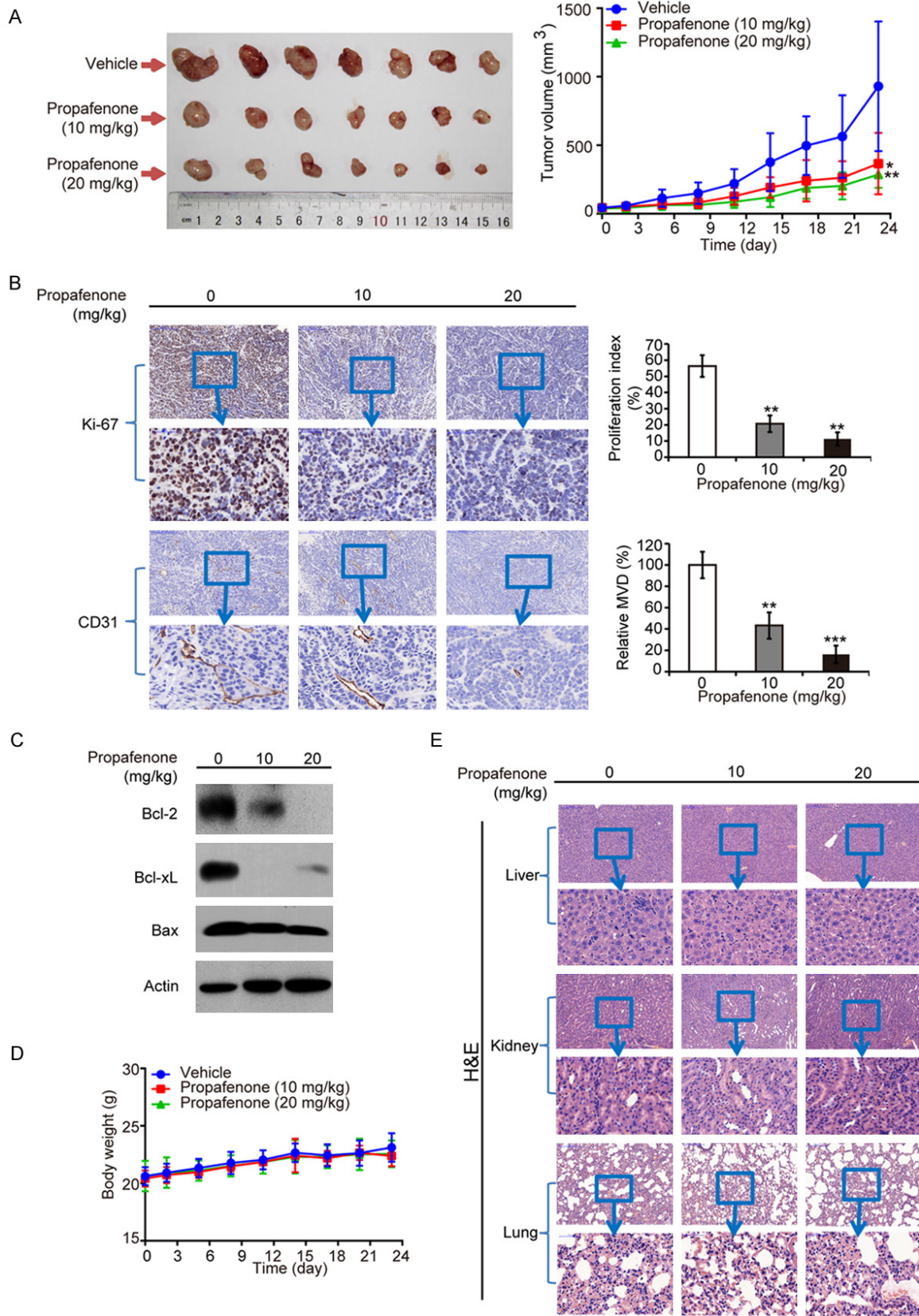
Figure 5. Propafenone suppresses tumor growth *in vivo*. Nude mice bearing KYSE270-derived xenografts were intraperitoneally injected with either propafenone (10 mg/kg or 20 mg/kg) or vehicle every other day (n = 7 per group). A.

Left, images of tumors; Right, tumor curves showed that propafenone exerted a significantly inhibitory effect on the growth of tumor xenografts. B. Immunohistochemical analysis of the Ki-67 proliferative index and CD31-based MVD. C. Expression levels of Bcl-xL, Bcl-2 and Bax in tumors from mice treated with propafenone or vehicle were detected by Western blot. D. Comparison of the body weight of nude mice during the experimental period. E. Representative images of liver, kidney and lungs stained with hematoxylin and eosin (H&E). Bars, SD; *, $P < 0.05$; **, $P < 0.01$; ***, $P < 0.001$ compared with the control group.

clinical treatment of arrhythmias according to current guidelines [31] and clinical studies [32, 33]. In addition to the data showing that propafenone did not exert any obvious toxic effects on normal esophageal epithelial cells or the vital organs of animals, we believe that propafenone could be a potential therapeutic drug for the management of ESCC.

With the rapid development of high-throughput technologies and computational frameworks, genetic alterations in human cancers and the mechanisms of action of anticancer drugs can be discovered more accurately and systematically. Mass spectrometry-based shotgun proteomics has been used to perform the data-dependent acquisition (DDA) mode of analysis, in which there is a priority of isolating and fragmenting more abundant precursor peptides to generate tandem mass (MS/MS) spectra [34]. However, the DIA mode has an advantage in the detection and quantification of both high and low abundance peptides, which leads to more complete quantitative coverage [10, 35]. In the DIA analysis mode, a set of wide windows is used to cover the entire mass range relevant to the researcher and to trigger the acquisition of fragment ion spectra for an unbiased set of precursors [36]. Recently, DIA-MS has been used to determine the biological mechanisms of human trabecular meshwork cells in response to dexamethasone and prednisolone, and the results showed that integrin cell surface interactions and other additional pathways were involved in corticosteroid-induced ocular hypertension [37]. In our study, we carried out DIA-MS to determine the potential mechanisms of how propafenone exerts an inhibitory effect on the proliferation of ESCC cells. As indicated by the proteomics data and IPA pathway analysis, a cluster of differentially expressed proteins was enriched in pathways related to mitochondrial dysfunction (**Figure 3**).

Mitochondria not only contain the components for energy production, including the TCA cycle and the core of the cellular respiratory chain and oxidative phosphorylation, but also play an important role in regulating cell apoptosis. In response to cellular and environmental alterations, the mitochondrial membrane equilibrium will be disturbed, and the permeabilization of outer membrane will increase, which leads to pro-apoptotic factors infiltrating the cytoplasm and inducing apoptosis. The anti-apoptotic proteins Bcl-2 and Bcl-xL engage the outer membrane to control mitochondrial permeability and suppress the release of apoptotic factors such as cytochrome C [38, 39]. One study showed that MT3-037, a novel microtubule inhibitor, could inactivate the pro-survival proteins Bcl-2 and Bcl-xL and activate the cleavage of caspases, resulting in the apoptosis of cancer cells [40]. It has reported that ABT-199 (navitoclax), a Bcl-2/Bcl-xL inhibitor, can cooperate with doxorubicin or dinaciclib to reduce Bcl-2 and Bcl-xL expression levels and activate mitochondria-mediated cell death in small cell lung cancer cells [41]. In the present study, our results indicated that propafenone downregulated the expression levels of Bcl-2 and Bcl-xL as well as disordered the equilibrium and damaged the polarity of mitochondria (**Figure 5**). Taken together, our data is the first evidence that propafenone may cause mitochondrial dysfunction by regulating Bcl-2 and Bcl-xL to therefore induce apoptosis and inhibit the proliferation of ESCC cells.

More than 50% of ESCC cases worldwide occur in China [42]. The incidence is still on the rise, and its overall survival rate remains low. Traditional chemotherapeutic drugs have many toxic side effects, such as toxic disturbance of the immune system, toxicity against human organs and myelosuppression [43]. Unfortunately, to date, there is no ideal targeted therapeutic drug for adjuvant treatment. All these obstacles compel us to develop new drugs or find new therapeutic regimens for cancer treatment. Nevertheless, the development of a completely new anticancer drug not only needs extensive time and cost but also elicits a higher treatment failure rate. Here, we demonstrated for the first time that propafenone, an FDA-approved antiarrhythmic medication, not only

triggered the intrinsic pathway of apoptosis mediated by mitochondria but also suppressed the growth of ESCC cells *in vitro* and *in vivo* accompanied by an inhibited Ki-67 proliferation index and reduced angiogenesis. Our data suggest that propafenone could be a novel treatment option for ESCC.

Acknowledgements

Disclosure of conflict of interest

None.

Address correspondence to: Qing-Yu He and Dr. Bin Li, Institute of Life and Health Engineering, College of Life Science and Technology, Jinan University, Guang-zhou 510632, China. Tel: 86-20-85227039; Fax: 86-20-85227039; E-mail: tqyhe@jnu.edu.cn (QYH); Tel: 86-20-85224372; Fax: 86-20-85224372; E-mail: libin2015@jnu.edu.cn (BL)

References

[1] Jemal A, Bray F, Center MM, Ferlay J, Ward E and Forman D. Global cancer statistics. CA Cancer J Clin 2011; 61: 69-90.

[2] Wheeler JB and Reed CE. Epidemiology of esophageal cancer. Surg Clin North Am 2012; 92: 1077-1087.

[3] Khaider NG, Lane D, Matte I, Rancourt C and Piche A. Targeted ovarian cancer treatment: the TRAILs of resistance. Am J Cancer Res 2012; 2: 75-92.

[4] Liu H, Lv L and Yang K. Chemotherapy targeting cancer stem cells. Am J Cancer Res 2015; 5: 880-893.

[5] Liu Q. Editorial: old drugs learn new tricks: Aadvances and applications for drug repurposing. Curr Top Med Chem 2016; 16: 3627-3628.

[6] Stoschitzky K, Klein W, Stark G, Stark U, Zernig G, Graziadei I and Lindner W. Different stereoselective effects of (R)- and (S)-propafenone: clinical pharmacologic, electrophysiologic, and radioligand binding studies. Clin Pharmacol Ther 1990; 47: 740-746.

[7] Alsaad AA, Ortiz Gonzalez Y, Austin CO and Kusumoto F. Revisiting propafenone toxicity. BMJ Case Rep 2017; 2017.

[8] Wang Y, Yu RY, Zhang J, Zhang WX, Huang ZH, Hu HF, Li YL, Li B and He QY. Inhibition of Nrf2 enhances the anticancer effect of 6-O-angeloylenolin in lung adenocarcinoma. Biochem Pharmacol 2017; 129: 43-53.

[9] Wang Y, Zhang J, Huang ZH, Huang XH, Zheng WB, Yin XF, Li YL, Li B and He QY. Isodeoxyelephantopin induces protective autophagy in lung cancer cells via Nrf2-p62-keap1 feedback loop. Cell Death Dis 2017; 8: e2876.

[10] Gillet LC, Navarro P, Tate S, Rost H, Selevsek N, Reiter L, Bonner R and Aebersold R. Targeted data extraction of the MS/MS spectra generated by data-independent acquisition: a new concept for consistent and accurate proteome analysis. Mol Cell Proteomics 2012; 11: O111. 016717.

[11] Hou G, Lou X, Sun Y, Xu S, Zi J, Wang Q, Zhou B, Han B, Wu L, Zhao X, Lin L and Liu S. Biomarker discovery and verification of esophageal squamous cell carcinoma using integration of SWATH/MRM. J Proteome Res 2015; 14: 3793-3803.

[12] Ernster L and Schatz G. Mitochondria: a historical review. J Cell Biol 1981; 91: 227s-255s.

[13] Trotta AP and Chipuk JE. Mitochondrial dynamics as regulators of cancer biology. Cell Mol Life Sci 2017; 74: 1999-2017.

[14] Kelly PN and Strasser A. The role of Bcl-2 and its pro-survival relatives in tumourigenesis and cancer therapy. Cell Death Differ 2011; 18: 1414-1424.

[15] Arbel N and Shoshan-Barmatz V. Voltage-dependent anion channel 1-based peptides interact with Bcl-2 to prevent antiapoptotic activity. J Biol Chem 2010; 285: 6053-6062.

[16] Zhong Y, Yang J, Xu WW, Wang Y, Zheng CC, Li B and He QY. KCTD12 promotes tumorigenesis by facilitating CDC25B/CDK1/Aurora A-dependent G2/M transition. Oncogene 2017; 36: 6177-6189.

[17] Wang Y, Huang ZH, Li YJ, He GW, Yu RY, Yang J, Liu WT, Li B and He QY. Dynamic quantitative proteomics characterization of TNF-alpha-induced necroptosis. Apoptosis 2016; 21: 1438-1446.

[18] Li B, Tsao SW, Chan KW, Ludwig DL, Novosyadlyy R, Li YY, He QY and Cheung AL. Id1-induced IGF-II and its autocrine/endocrine promotion of esophageal cancer progression and chemoresistance--implications for IGF-II and IGF-IR-targeted therapy. Clin Cancer Res 2014; 20: 2651-2662.

[19] Li B, Xu WW, Guan XY, Qin YR, Law S, Lee NP, Chan KT, Tam PY, Li YY, Chan KW, Yuen HF, Tsao SW, He QY and Cheung AL. Competitive binding between Id1 and E2F1 to Cdc20 regu-

lates E2F1 degradation and thymidylate synthase expression to promote esophageal cancer chemoresistance. Clin Cancer Res 2016; 22: 1243-1255.

[20] Li B, Xu WW, Han L, Chan KT, Tsao SW, Lee NPY, Law S, Xu LY, Li EM, Chan KW, Qin YR, Guan XY, He QY and Cheung ALM. MicroRNA-377 suppresses initiation and progression of esophageal cancer by inhibiting CD133 and VEGF. Oncogene 2017; 36: 3986-4000.

[21] Xu WW, Li B, Guan XY, Chung SK, Wang Y, Yip YL, Law SY, Chan KT, Lee NP, Chan KW, Xu LY, Li EM, Tsao SW, He QY and Cheung AL. Cancer cell-secreted IGF2 instigates fibroblasts and bone marrow-derived vascular progenitor cells to promote cancer progression. Nat Commun 2017; 8: 14399.

[22] Pavelka N, Pelizzola M, Vizzardelli C, Capozzoli M, Splendiani A, Granucci F and Ricciardi-Castagnoli P. A power law global error model for the identification of differentially expressed genes in microarray data. BMC Bioinformatics 2004; 5: 203.

[23] Zhang Z, Zheng Y, Zhu R, Zhu Y, Yao W, Liu W and Gao X. The ERK/eIF4F/Bcl-XL pathway mediates SGP-2 induced osteosarcoma cells apoptosis in vitro and in vivo. Cancer Lett 2014; 352: 203-213.

[24] Boucher MJ, Morisset J, Vachon PH, Reed JC, Laine J and Rivard N. MEK/ERK signaling pathway regulates the expression of Bcl-2, Bcl-X(L), and Mcl-1 and promotes survival of human pancreatic cancer cells. J Cell Biochem 2000; 79: 355-369.

[25] Valderrabano M and Singh BN. Electrophysiologic and antiarrhythmic effects of propafenone: focus on atrial fibrillation. J Cardiovasc Pharmacol Ther 1999; 4: 183-198.

[26] Capucci A, Villani GQ, Aschieri D and Piepoli M. Safety of oral propafenone in the conversion of recent onset atrial fibrillation to sinus rhythm: a prospective parallel placebo-controlled multicentre study. Int J Cardiol 1999; 68: 187-196.

[27] Hancox JC and Mitcheson JS. Inhibition of L-type calcium current by propafenone in single myocytes isolated from the rabbit atrioventricular node. Br J Pharmacol 1997; 121: 7-14.

[28] Lee JT, Kroemer HK, Silberstein DJ, Funck-Brentano C, Lineberry MD, Wood AJ, Roden DM and Woosley RL. The role of genetically determined polymorphic drug metabolism in the beta-blockade produced by propafenone. N Engl J Med 1990; 322: 1764-1768.

[29] McLeod AA, Stiles GL and Shand DG. Demonstration of beta adrenoceptor blockade by propafenone hydrochloride: clinical pharmacologic, radioligand binding and adenylate cyclase activation studies. J Pharmacol Exp Ther 1984; 228: 461-466.

[30] Stoschitzky K, Stoschitzky G, Lercher P, Brussee H, Lamprecht G and Lindner W. Propafenone shows class Ic and class II antiarrhythmic effects. Europace 2016; 18: 568-571.

[31] Camm AJ, Lip GY, De Caterina R, Savelieva I, Atar D, Hohnloser SH, Hindricks G, Kirchhof P; ESC Committee for Practice Guidelines-CPG; Document Reviewers. 2012 focused update of the ESC guidelines for the management of atrial fibrillation: an update of the 2010 ESC guidelines for the management of atrial fibrillation--developed with the special contribution of the European heart rhythm association. Europace 2012; 14: 1385-1413.

[32] Bellandi F, Simonetti I, Leoncini M, Frascarelli F, Giovannini T, Maioli M and Dabizzi RP. Long-term efficacy and safety of propafenone and sotalol for the maintenance of sinus rhythm after conversion of recurrent symptomatic atrial fibrillation. Am J Cardiol 2001; 88: 640-645.

[33] Freemantle N, Lafuente-Lafuente C, Mitchell S, Eckert L and Reynolds M. Mixed treatment comparison of dronedarone, amiodarone, sotalol, flecainide, and propafenone, for the management of atrial fibrillation. Europace 2011; 13: 329-345.

[34] Teo G, Kim S, Tsou CC, Collins B, Gingras AC, Nesvizhskii AI and Choi H. mapDIA: preprocessing and statistical analysis of quantitative proteomics data from data independent acquisition mass spectrometry. J Proteomics 2015; 129: 108-120.

[35] Canterbury JD, Merrihew GE, MacCoss MJ, Goodlett DR and Shaffer SA. Comparison of data acquisition strategies on quadrupole ion trap instrumentation for shotgun proteomics. J Am Soc Mass Spectrom 2014; 25: 2048-2059.

[36] Venable JD, Dong MQ, Wohlschlegel J, Dillin A and Yates JR. Automated approach for quantitative analysis of complex peptide mixtures from tandem mass spectra. Nat Methods 2004; 1: 39-45.

[37] Shan SW, Do CW, Lam TC, Kong RPW, Li KK, Chun KM, Stamer WD and To CH. New insight of common regulatory pathways in human trabecular meshwork cells in response to dexamethasone and prednisolone using an integrated quantitative proteomics: SWATH and MRM-HR mass spectrometry. J Proteome Res 2017; 16: 3753-3765.

[38] Lopez J and Tait SW. Mitochondrial apoptosis: killing cancer using the enemy within. Br J Cancer 2015; 112: 957-962.

[39] Vyas S, Zaganjor E and Haigis MC. Mitochondria and cancer. Cell 2016; 166: 555-566.

[40] Chang LC, Yu YL, Hsieh MT, Wang SH, Chou RH, Huang WC, Lin HY, Hung HY, Huang LJ and Kuo SC. A novel microtubule inhibitor, MT3-037, causes cancer cell apoptosis by inducing mi-

totic arrest and interfering with microtubule dynamics. Am J Cancer Res 2016; 6: 747-763.

[41] Inoue-Yamauchi A, Jeng PS, Kim K, Chen HC, Han S, Ganesan YT, Ishizawa K, Jebiwott S, Dong Y, Pietanza MC, Hellmann MD, Kris MG, Hsieh JJ and Cheng EH. Targeting the differential addiction to anti-apoptotic BCL-2 family for cancer therapy. Nat Commun 2017; 8: 16078.

[42] Zeng H, Zheng R, Zhang S, Zuo T, Xia C, Zou X and Chen W. Esophageal cancer statistics in China, 2011: estimates based on 177 cancer registries. Thorac Cancer 2016; 7: 232-237.

[43] Tacar O, Sriamornsak P and Dass CR. Doxorubicin: an update on anticancer molecular action, toxicity and novel drug delivery systems. J Pharm Pharmacol 2013; 65: 157-170.

Supplementary Table 1. Differently expressed proteins in the propafenone-treated KYSE270 cells

Protein name	Accession ID	Fold change	P value
ILVBL	A1L0T0	0.597204757	0.036947481
NBAS	A2RRP1	2.209296148	0.019374062
C5orf51	A6NDU8	1.625030904	0.045963558
TUBAL3	A6NHL2	0.280062216	0.00037299
UNC119B	A6NIH7	1.632852882	0.043325473
SNRPGP15; SNRPG	A8MWD9	2.274000834	0.004180064
NACA	E9PAV3	1.504809488	0.013034655
MYL3	O00249	1.383725376	0.007416935
PDLIM1	O00151	0.58282821	0.010347981
SNAP23	O00161	2.89369575	0.035492676
STXBP3	O00186	1.564661142	0.010582351
NDUFS8	O00217	0.48428277	0.016222937
PGRMC1	O00264	1.511080312	0.022943909
CLIC1	O00299	0.713507066	0.023449804
GOLIM4	O00461	2.010094306	0.048735977
NDUFA4	O00483	1.342147611	0.04639657
NOP56	O00567	0.646526125	0.042819578
PIR	O00625	1.539328849	0.017357628
MAN2B1	O00754	1.814265116	0.003499821
AP3D1	O14617	0.251805428	0.020301536
PDCD5	O14737	2.060071063	0.002526617
MGST3	O14880	0.120912411	0.013331904
HNRNPDL	O14979	1.799337501	0.033340479
XPO1	O14980	0.684502015	0.00193069
SEC16A	O15027	0.150246376	0.041654877
PFAS	O15067	1.507456789	0.01620293
NPC1	O15118	1.762024212	0.032301536
PGRMC2	O15173	1.400770655	0.033346195
PFDN6	O15212	1.505945256	0.008797428
STX7	O15400	2.22570502	0.03117542
CD3EAP	O15446	0.462194232	0.048298678
TTI1	O43156	1.667371864	0.031008217
PHGDH	O43175	1.320773874	0.018806717
ERI3	O43414	2.219502212	0.016896034
PPIH	O43447	1.922835585	0.027664166
GSTZ1	O43708	0.601266266	0.014233655
ENSA	O43768	0.453819915	0.022420865
AKAP8	O43823	1.980386849	0.003596999
TIMM8A	O60220	3.18812249	0.045627724
KDM1A	O60341	1.546795463	0.009782065
RANBP6	O60518	0.542698325	0.011964273
ATP6V1G1	O75348	1.945127172	0.01948696
SH3BGRL	O75368	1.98239447	0.00706681
BANF1	O75531	2.25354579	0.013423365
RPS6KA4	O75676	1.8548738	0.012380136
ADAP1; ADAP2	O75689	0.427690778	0.030478028
RP2	O75695	0.476063938	0.027684173
DNAJC8	O75937	1.95446511	0.044791711
CPD	O75976	0.610620692	0.048608789
MYO1D	O94832	1.654570873	0.029390497
AKR7A3	O95154	1.531201701	0.03657592
RTN3	O95197	1.377274732	0.018806717
SMC2	O95347	0.526608944	0.021643444

ETHE1	O95571	1.730521346	0.025674884
TXNDC12	O95881	1.711198276	0.04701965
MT-CO2	P00403	0.66675259	0.018776706
PLG	P00747	1.788413754	0.004876027
KRT14	P02533	2.433133867	0.008608789
KRT6A	P02538	1.794507151	0.021243301
APOE	P02649	1.357651801	0.030052161
APOC3	P02656	1.423184685	0.006347981
RBP4	P02753	0.501371518	0.026989639
GC	P02774	0.771783301	0.021107538
TFRC	P02786	0.675832805	0.00611647
LTF	P02788	0.762368635	0.001903537
VTN	P04004	0.584298999	0.036665952
ALDOA	P04075	1.277895108	0.021424795
PRNP	P04156	1.825018251	0.008141479
KRT6B	P04259	1.736525489	0.013923544
KRT1	P04264	1.581041776	0.001669168
TUBB4A	P04350	2.746928476	0.041013219
HIST1H2AB; HIST1H2AC; HIST1H2AD; HIST1H2AH; HIST1H2AJ; HIST1H2AG; HIST3H2A; H2AFJ	P04908	0.804353113	0.035156842
SLC25A5	P05141	0.805236718	0.014323687
PCCB	P05166	2.257046215	0.015172562
EIF2S1	P05198	0.680264152	0.027262594
HMGN2	P05204	1.988105282	0.00309682
RPLP2	P05387	2.069940457	0.023801358
SERPINA7	P05543	0.678853276	0.037666309
TPM3	P06753	1.238854528	0.012493033
CTSD	P07339	0.611118715	0.021496249
CTSL	P07711	1.854454956	0.00560343
PFN1	P07737	1.678034693	0.007969989
CYC1	P08574	1.757080876	0.034720972
KRT16	P08779	5.306537989	0.002143623
CD63	P08962	0.256623319	0.001766345
SRP19	P09132	1.620931618	0.029892104
HMGB1	P09429	1.432385715	0.022529475
HNRNPA1	P09651	1.548785771	0.013541979
UCHL1	P09936	1.34959109	0.030965345
LAMP1	P11279	1.332969578	0.033947839
ADH5	P11766	0.694265823	0.034110754
PABPC1	P11940	1.321489759	0.043931404
TPR	P12270	0.651632588	0.04054448
CKMT1A	P12532	0.330314323	0.00133905
LAMP2	P13473	1.355765563	0.036943194
MTHFD2	P13995	1.999652794	0.008118614
MIF	P14174	2.612744466	0.000190068
SNRPB; SNRPN	P14678	1.398736926	0.036214362
UQCRB	P14927	3.270231798	0.003985709
NQO1	P15559	1.299519409	0.04831154
ACADS	P16219	2.072695582	0.019869954
HIST1H1B	P16401	1.220900441	0.032408717
YBX3	P16989	0.629240666	0.031082529
HSPA6	P17066	1.508608068	0.002579493
PRKCA	P17252	1.825803742	0.047748482
RPL35A	P18077	1.369335281	0.041799214
ATP5J	P18859	2.089981982	0.012841729
XRCC1	P18887	0.620724166	0.041434798
EIF2S2	P20042	1.515215054	0.022413719
BTF3	P20290	1.43737354	0.04093462

Gene	Accession	Value 1	Value 2
PSMB1	P20618	0.762851349	0.043982851
M6PR	P20645	1.531626592	0.038062165
PTMS	P20962	2.73955042	0.006002144
NME2	P22392	1.561694603	0.006633798
FDXR	P22570	1.649591125	0.01578135
HNRNPA2B1	P22626	1.487821904	0.020250089
PPIB	P23284	1.347159768	0.02136906
GCSH	P23434	1.501727462	0.03732333
EEF1B2	P24534	1.303162958	0.041956413
ATP5F1	P24539	0.523667796	0.014109325
ACP1	P24666	1.435917782	0.026955341
RPS12	P25398	3.199511614	0.001969275
PSMA1	P25786	1.584276238	0.022192212
CTNNA2	P26232	0.450834305	0.008577349
EEF1G	P26641	0.793426015	0.041954984
FKBP2	P26885	1.613432756	0.026843873
RPL10	P27635	1.389432697	0.026720972
RPA1	P27694	0.665464512	0.039552697
ABCD3	P28288	0.582966896	0.027209718
GRN	P28799	0.177837389	0.001363344
S100A2	P29034	0.821989148	0.032315827
ERP29	P30040	1.363286611	0.033121829
C21 or f33	P30042	2.102385911	0.009300464
PRDX5	P30044	1.453040322	0.033404787
ATP5D	P30049	1.765283064	0.010050732
CMPK1	P30085	1.495495038	0.036971776
PEBP1	P30086	1.705337441	0.012322972
STIP1	P31948	1.313010603	0.034952483
PRDX2	P32119	1.243743836	0.04831154
DUT	P33316	1.687447471	0.024836013
HIST1H2BB; HIST1H2BJ; HIST1H2BO; HIST2H2BE; HIST3H2BB	P33778	1.548066941	0.008160057
GPC1	P35052	0.678337727	0.049221865
RPL22	P35268	1.312547419	0.030616649
KRT9	P35527	1.842915011	0.016976063
KRT2	P35908	1.422637313	0.0376806
ATP6V1E1	P36543	1.973623876	0.005294748
LONP1	P36776	4.52559771	0.002022151
TAGLN2	P37802	1.260832245	0.044228653
RBMX	P38159	2.003446267	0.011895677
CAPG	P40121	1.977481118	0.008657378
NAA10	P41227	2.144790108	0.015709896
RPS27	P42677	0.6887122	0.029806359
CDKN2A; CDKN2B	P42771	3.37451866	0.004533048
PPIC	P45877	1.416885233	0.048490175
CRK	P46108	2.01583502	0.01758771
CRKL	P46109	1.633632639	0.030903894
NSF	P46459	1.664074653	0.016088603
RPL21	P46778	1.305730245	0.049406217
RPS9	P46781	0.644217635	0.007895677
CAPZA2	P47755	1.591709642	0.032397285
EIF1AX	P47813	1.377284396	0.034953912
RPL29	P47914	0.623992328	0.006966774
PSMD8	P48556	1.508076506	0.039129689
PRRC2A	P48634	0.449461539	0.028555913
CD97	P48960	0.602108454	0.040714541
RPL34	P49207	1.551491871	0.023165416

RPIA	P49247	0.614497549	0.044384423
MCM2	P49736	2.131229646	0.004758842
MRE11A	P49959	4.131123895	0.000733119
PPT1	P50897	0.369037746	0.003435513
ALDH3A2	P51648	0.602481241	0.034769561
ARHGDIB	P52566	1.886594915	0.015912826
NUBP1	P53384	1.817784526	0.033330475
SUB1	P53999	1.948370368	0.004936049
AK2	P54819	1.471748999	0.033576277
NAP1L1	P55209	0.725705527	0.026483744
CASP7	P55210	0.365729079	0.006669525
ATP5I	P56385	1.799921164	0.013098964
C21 or f59	P57076	0.220235112	0.004344409
RAB25	P57735	0.330946859	0.007179707
SEC61G	P60059	0.701818018	0.014765273
TPI1	P60174	1.293219049	0.025594855
MYL6	P60660	1.310125679	0.045184709
S100A10	P60903	1.457229549	0.011647017
GMFB	P60983	1.54681555	0.027214005
RAB10	P61026	1.619004881	0.016475884
RPL26	P61254	1.579103452	0.012931761
PCBD1	P61457	3.547328819	0.004744552
RPL37A	P61513	2.382762002	0.005299035
HSPE1	P61604	1.97646982	0.004883173
B2M	P61769	1.39933099	0.042502322
COPZ1	P61923	0.701032522	0.027158271
RPS18	P62269	1.428301616	0.014668096
RPS11	P62280	1.738904003	0.00451304
SNRPF	P62306	1.393997933	0.045341908
SNRPD1	P62314	0.739131846	0.036180064
ACTA2; ACTG2	P62736	0.769646958	0.013772061
RPL23A	P62750	0.666922507	0.017091819
VSNL1	P62760	0.619471039	0.042436584
HIST1H2BC; HIST1H2BD; HIST1H2BH; HIST1H2BK; HIST1H2BL; HIST1H2BM; HIST1H2BN; HIST2H2BF; H2BFS	P62807	1.581880487	0.013126116
RAN	P62826	1.194672516	0.047514112
UBE2D2; UBE2D3	P62837	1.496288538	0.03458378
RPS15	P62841	0.716065378	0.02683244
FAU	P62861	0.766825081	0.031531261
RPL31	P62899	0.783012774	0.041889246
RPL32	P62910	1.48742485	0.016474455
RPL8	P62917	1.483689689	0.020760272
PPIA	P62937	1.735846099	0.00155627
GRB2	P62993	1.651421843	0.025903537
TRA2B	P62995	1.573684139	0.025719185
RPL38	P63173	1.792038708	0.048440157
UBE2L3	P68036	2.133746055	0.006155055
TUBA4A	P68366	0.806320654	0.0294791
HIST1H3A	P68431	0.399513167	0.005434798
HBA1	P69905	1.259840395	0.027504109
IGBP1	P78318	0.518169874	0.029423365
RAE1	P78406	2.261726428	0.012577349
ERH	P84090	2.154482779	0.014931047
H3F3A	P84243	0.695915059	0.039975706
PURA	Q00577	1.698496472	0.022442301
FABP5	Q01469	2.306826102	0.004441586

IFITM3	Q01628	1.832179432	0.011801358
SLC7A5	Q01650	0.691605278	0.030216506
DR1	Q01658	1.712369158	0.020811718
BDH1	Q02338	1.80656764	0.036914612
CAV1	Q03135	0.486187088	0.007745623
TAP2	Q03519	0.547761661	0.015412647
KRT17	Q04695	1.820651601	0.033393355
GLO1	Q04760	1.493503889	0.014682387
PLP2	Q04941	2.27817697	0.004873169
SRSF11	Q05519	0.70357139	0.048548767
EEF1A2	Q05639	0.694166653	0.018245088
PTPN11	Q06124	0.125229704	0.000714541
FMR1	Q06787	1.755561162	0.02963487
DDR1	Q08345	0.48213341	0.037822079
GOLGA2	Q08379	1.866602161	0.037153269
PPID	Q08752	1.592542456	0.033341908
ASPH	Q12797	0.61603182	0.002622365
CSTF3	Q12996	0.580409511	0.009048946
FLII	Q13045	0.599040727	0.036587353
GPS1	Q13098	0.607043208	0.030652376
PRDX4	Q13162	0.71957984	0.04493319
SRSF6	Q13247	1.653226765	0.015172562
G3BP1	Q13283	1.390795317	0.03984423
IFIT5	Q13325	0.56400687	0.020605931
SQSTM1	Q13501	1.556059611	0.039282601
PIN1	Q13526	2.317035367	0.033429082
CUL4B	Q13620	2.135339636	0.010375134
CBFB	Q13951	1.979178651	0.022400857
COTL1	Q14019	0.583545496	0.024423008
TRIM29	Q14134	1.59866776	0.014482315
SCRIB	Q14160	2.626115659	0.037046088
MLEC	Q14165	2.167152619	0.013128975
MAP7	Q14244	0.493916459	0.006745266
GNA13	Q14344	0.721194401	0.019925688
WFDC2	Q14508	0.379547691	0.028310111
LAGE3	Q14657	0.556770311	0.042092176
PPP2R5D	Q14738	0.456794396	0.042938192
LBR	Q14739	0.611036338	0.005622008
CASP8	Q14790	0.621315134	0.022313683
NAA25	Q14CX7	0.619740446	0.03922115
ARL6IP1	Q15041	2.220937542	0.040507324
EIF4H	Q15056	1.315331085	0.013240443
RAB35	Q15286	0.720496742	0.036754555
DHCR24	Q15392	0.642257732	0.029959271
CNN3	Q15417	1.471921899	0.038450875
SF3A2	Q15428	1.67062798	0.043189711
MAPRE2	Q15555	0.678641186	0.039788496
TRAM1	Q15629	0.486231622	0.028191497
MAPRE1	Q15691	0.732478216	0.020853162
ADRM1	Q16186	0.682465782	0.044315827
CCDC6	Q16204	1.997910159	0.036180064
BAK1	Q16611	0.411664146	0.025864952
NDUFA5	Q16718	1.785155729	0.009173276
HADH	Q16836	0.641726315	0.025547696
UGT8	Q16880	0.458017925	0.027759914
ERCC6L	Q2NKX8	0.614217143	0.032831726

Gene	ID	Value 1	Value 2
UAP1L1	Q3KQV9	2.642838731	0.041639157
CCDC58	Q4VC31	1.573017508	0.013168989
USP39	Q53GS9	0.630245846	0.041859235
COQ5	Q5HYK3	0.528776027	0.023599857
AARS2	Q5JTZ9	1.76886134	0.014040729
NUP188	Q5SRE5	0.515095581	0.023761343
UBR4	Q5T4S7	0.422970459	0.021756342
RBM26	Q5T8P6	1.713352319	0.009048946
EMC10	Q5UCC4	2.49329507	0.026262237
PRPF38B	Q5VTL8	0.268707392	0.011021079
ARHGAP17	Q68EM7	1.607933463	0.003451233
AGTRAP	Q6RW13	0.679421189	0.032567345
HIST2H3A	Q71DI3	0.550102049	0.04493319
HS2ST1	Q7LGA3	1.559412258	0.024110039
ATG9A	Q7Z3C6	0.576747588	0.042652376
CLASP1	Q7Z460	0.390527543	0.038239371
HDDC2	Q7Z4H3	2.28231198	0.007379778
KIF21A	Q7Z4S6	0.561783427	0.013923544
LSR	Q86X29	1.910574479	0.0196413
PHF6	Q8IWS0	0.48224863	0.038216506
DNAJC10	Q8IXB1	1.715991482	0.012648803
SRRM1	Q8IYB3	0.304331396	0.045719185
VKORC1L1	Q8N0U8	0.457582146	0.004785995
EHBP1L1	Q8N3D4	0.461607135	0.007599857
CISD2	Q8N5K1	1.666522392	0.022578064
SUMF2	Q8NBJ7	0.697408789	0.037077528
SPC24	Q8NBT2	0.40890974	0.042603787
NUP37	Q8NFH4	0.62976347	0.005497678
ATL2	Q8NHH9	1.682674442	0.039399786
THOC2	Q8NI27	1.957103562	0.035189711
FAM213B	Q8TBF2	1.711182335	0.034656663
TBC1D15	Q8TC07	0.461449244	0.049106109
NUP210	Q8TEM1	0.659959649	0.013729189
ZC3H15	Q8WU90	2.167342366	0.04094891
CHMP7	Q8WUX9	0.643026658	0.013423365
NUDCD2	Q8WVJ2	1.633552166	0.048658807
GATAD2B	Q8WXI9	1.890257161	0.033056091
CTNNBL1	Q8WYA6	0.425865703	0.033956413
MRPS31	Q92665	0.595537621	0.01912826
AKAP1	Q92667	4.052363138	0.041327617
PRCC	Q92733	0.340050389	0.010387996
OSTF1	Q92882	1.548973548	0.009579135
GPKOW	Q92917	1.817726337	0.037894962
RAB8B	Q92930	1.935728256	0.039568417
LPP	Q93052	0.637415918	0.027306895
TSR2	Q969E8	0.471974864	0.047215434
UBE2E3; UBE2E2	Q969T4	0.656143355	0.005912111
PSMG2	Q969U7	0.575925545	0.033939264
TBRG4	Q969Z0	0.626092091	0.02502751
FAM162A	Q96A26	0.638288742	0.027029653
CCDC124	Q96CT7	1.533771004	0.03246731
NMD3	Q96D46	0.690575344	0.042266524
HOOK2	Q96ED9	0.370125443	0.043056806
CCDC126	Q96EE4	1.911964327	0.019039657
SAAL1	Q96ER3	1.787402313	0.036060021
PTCD3	Q96EY7	0.673224371	0.028503037

EDC3	Q96F86	0.590181358	0.039737049
SCRN2	Q96FV2	1.757424027	0.004
REEP6	Q96HR9	1.941303951	0.037754912
PGAM5	Q96HS1	0.683465377	0.01849089
SUCLG2	Q96I99	2.170255172	0.041329046
ITCH	Q96J02	0.65281696	0.009274741
CDK5RAP3	Q96JB5	3.557821539	0.048254377
NACC1	Q96RE7	0.43383782	0.0014005
MYADM	Q96S97	0.538674021	0.036142908
PSMB7	Q99436	1.380119284	0.028724544
CNN2	Q99439	1.624708259	0.049096106
PFDN5	Q99471	1.722927384	0.02667667
PARK7	Q99497	1.766714039	0.014403716
EYA3	Q99504	0.518837863	0.010550911
SORT1	Q99523	0.645192719	0.040896034
LGMN	Q99538	0.626474159	0.049970704
TXN2	Q99757	3.060058745	0.029411933
SLC29A1	Q99808	2.494742607	0.010172204
ARPC5L	Q9BPX5	1.505899327	0.021376206
MACROD1	Q9BQ69	3.839311592	0.049319043
WDR77	Q9BQA1	0.665041712	0.006269382
TXNDC17	Q9BRA2	2.5833483	0.031172562
C7 or f50	Q9BRJ6	0.528770257	0.004573062
TMEM70	Q9BUB7	0.590793721	0.007512683
EMC6	Q9BV81	1.827094128	0.013098964
SARG	Q9BW04	0.499615837	0.005294748
LSM14B	Q9BX40	1.646368673	0.035152554
HINT2	Q9BX68	2.661455112	0.043415506
OSBPL10	Q9BXB5	0.561528262	0.011371204
AP1M1	Q9BXS5	1.463659495	0.014993926
NUSAP1	Q9BXS6	0.371339805	0.042845302
C14 or f142	Q9BXV9	2.230572575	0.049480529
GNB1L	Q9BYB4	1.550593325	0.014610932
NLN	Q9BYT8	0.402398158	0.032951768
MRPL37	Q9BZE1	0.645585322	0.006333691
UBL5	Q9BZL1	3.52100151	0.039955698
WDR12	Q9GZL7	0.554096056	0.003614148
TMEM126A	Q9H061	1.69643643	0.031861379
RAB6C	Q9H0N0	0.304524939	0.046639514
NUCKS1	Q9H1E3	1.750213512	0.008810289
MRPL46	Q9H2W6	0.448346249	0.048717399
POFUT1	Q9H488	1.528882258	0.014440872
PIGU	Q9H490	1.503255744	0.034155055
RANBP3	Q9H6Z4	0.543227789	0.038663809
C17orf75	Q9HAS0	1.514775313	0.0282801
RDH14	Q9HBH5	0.552106499	0.042072169
DYNLRB1	Q9NP97	1.824178038	0.034946767
ISYNA1	Q9NPH2	0.728736336	0.021934977
RTN4	Q9NQC3	0.654375077	0.047485531
POLE3	Q9NRF9	1.576072077	0.021902108
UBQLN4	Q9NRR5	0.426906548	0.037942122
HEBP1	Q9NRV9	2.19908934	0.01402358
PLSCR3	Q9NRY6	70.91640158	0.009269025
EXOC1	Q9NV70	1.975464889	0.000364416
UQCC1	Q9NVA1	0.599346047	0.012161486
EXD2	Q9NVH0	0.586586996	0.030859593

DNAJC11	Q9NVH1	0.573701998	0.035086817
FANCI	Q9NVI1	0.518191217	0.018479457
NDUFB11	Q9NX14	0.636394177	0.018136477
CHCHD3	Q9NX63	1.586861462	0.033823508
TVP23B	Q9NYZ1	2.692056958	0.039281172
CISD1	Q9NZ45	2.076237056	0.009423365
COQ3	Q9NZJ6	1.955198986	0.020838871
EMC3	Q9P0I2	1.5137619	0.027278314
NDUFA13	Q9P0J0	1.437136782	0.046257949
PDP1	Q9P0J1	2.203864658	0.027381208
ABRACL	Q9P1F3	2.201649215	0.005220436
CAMSAP3	Q9P1Y5	0.528132175	0.006569489
GMPR2	Q9P2T1	1.784573674	0.047394069
METTL1	Q9UBP6	1.719813808	0.04740836
PEF1	Q9UBV8	0.688813091	0.030946767
SLC25A10	Q9UBX3	3.211806872	0.038995355
PFDN2	Q9UHV9	2.633878402	0.011113969
ENOPH1	Q9UHY7	0.659252626	0.00356413
ATP6V1H	Q9UI12	0.5768089	0.046733834
LCMT1	Q9UIC8	0.595976935	0.020272955
LNPEP	Q9UIQ6	2.833265414	0.030429439
VPS28	Q9UK41	1.583124894	0.014986781
LSM7	Q9UK45	6.055300136	0.014659521
G3BP2	Q9UN86	1.576626139	0.004565916
EXOC6B	Q9Y2D4	1.810303672	0.038935334
LAMTOR2	Q9Y2Q5	0.328242904	0.042336549
POLDIP2	Q9Y2S7	0.637095107	0.00896463
DHRS7	Q9Y394	0.611074274	0.031628439
TMED5	Q9Y3A6	0.666981338	0.026252233
FIS1	Q9Y3D6	1.999298753	0.024138621
FBXO7	Q9Y3I1	0.573348002	0.012157199
RABGAP1	Q9Y3P9	0.58646577	0.029376206
RPL36	Q9Y3U8	0.715158894	0.045289032
MAP4K5	Q9Y4K4	3.069250543	0.013997856
NPTN	Q9Y639	2.295002724	0.010949625
SPCS1	Q9Y6A9	0.646490492	0.01184423
MAD1L1	Q9Y6D9	0.61680975	0.039069668
NDUFB9	Q9Y6M9	1.538444161	0.028707395
UB2V1_HUMAN; UB2V2_HUMAN	Q13404	1.309435665	0.034535191